

Slow-Wave Hybrid Magnonics

Jing Xu,¹ Changchun Zhong², Shihao Zhuang,³ Chen Qian,⁴ Yu Jiang,⁵ Amin Pishehvar,⁵ Xu Han,¹ Dafei Jin,^{6,1} Josep M. Jornet⁵, Bo Zhen,⁴ Jiamian Hu,³ Liang Jiang², and Xufeng Zhang^{5,7,*}

¹Center for Nanoscale Materials, Argonne National Laboratory, Lemont, Illinois 60439, USA

²Pritzker School of Molecular Engineering, University of Chicago, Chicago, Illinois 60637, USA

³Department of Materials Science and Engineering, University of Wisconsin—Madison, Madison, Wisconsin 53706, USA

⁴Department of Physics and Astronomy, University of Pennsylvania, Philadelphia, Pennsylvania 19104, USA

⁵Department of Electrical and Computer Engineering, Northeastern University, Boston, Massachusetts 02115, USA

⁶Department of Physics and Astronomy, University of Notre Dame, Notre Dame, Indiana 46556, USA

⁷Department of Physics, Northeastern University, Boston, Massachusetts 02115, USA



(Received 18 May 2023; revised 14 December 2023; accepted 8 February 2024; published 12 March 2024)

Cavity magnonics is an emerging research area focusing on the coupling between magnons and photons. Despite its great potential for coherent information processing, it has been long restricted by the narrow interaction bandwidth. In this Letter, we theoretically propose and experimentally demonstrate a novel approach to achieve broadband photon-magnon coupling by adopting slow waves on engineered microwave waveguides. To the best of our knowledge, this is the first time that slow wave is combined with hybrid magnonics. Its unique properties promise great potentials for both fundamental research and practical applications, for instance, by deepening our understanding of the light-matter interaction in the slow wave regime and providing high-efficiency spin wave transducers. The device concept can be extended to other systems such as optomagnonics and magnomechanics, opening up new directions for hybrid magnonics.

DOI: [10.1103/PhysRevLett.132.116701](https://doi.org/10.1103/PhysRevLett.132.116701)

Cavity magnonics is an emerging area exploring the utilization of magnons—quasiparticles describing collective spin excitations known as spin waves—for coherent information processing [1–6]. Different from conventional magnonics [7,8], cavity magnonics focuses on coherent interaction between magnons and cavity photons instead of the magnonic dynamics itself. Such interaction allows coherent information exchange between magnons and photons, leading to coherent phenomena including strong coupling [9–15], magnetically induced transparency [10], and unidirectional invisibility [16,17], which enable wide applications in quantum transduction [18,19], dark matter detection [20,21], and neuromorphic computing [22].

In cavity magnonics, the magnon-photon coupling can be significantly enhanced via photon recycling at resonances. Through proper cavity design, the magnon-photon coupling strength can surpass system dissipation levels, enabling an efficient and robust interaction between the two modes. For instance, at microwave frequencies, metallic three-dimensional cavities or coplanar waveguide (CPW) resonators are often used to host magnonic resonators, allowing the observation of strong [9–15] and even ultra-strong [10,23,24] photon-magnon coupling. When coupling magnons with optical photons or mechanical phonons where the interaction is intrinsically weak, complicated triple-resonance conditions can be applied to achieve further interaction enhancement [25–28].

Despite the enhanced coupling, cavity magnonics suffers from its finite bandwidth. Although the magnon frequency

is widely tunable, the coherent magnon-photon coupling can only be observed near the fixed cavity frequency. Within the limited exploration of broadband magnon-photon coupling, only cascaded discrete features are obtained [29], which remains inherently narrow band. Such small bandwidths complicate device designs and limit applications of cavity magnonics. To break this restriction, nonresonant structures supporting broadband traveling photons are desired. However, the interaction of traveling photons with magnons is usually weak. Particularly, it is extremely challenging to detect magnon signals on integrated devices where micro- or nanomagnonic resonators are coupled with microstrips or CPWs, which usually requires sophisticated technologies such as Brillouin light scattering [30] that are expensive and incompatible with large-scale device integration.

To address this challenge, we propose a novel concept of slow-wave hybrid magnonics. It originates from previous demonstrations in optical domain where slow lights—traveling optical photons with reduced group velocities—are used to enhance light-matter interactions and enable new functionalities without compromising the bandwidth [31–34]. By introducing spoof surface plasmon polariton (SSPP) structures [35–38], slow waves can also be obtained for microwave photons with largely reduced group velocities. SSPP has experienced rapid development in the past decades and found wide applications in developing compact microwave or THz devices. Here, for the first time, we combine the two promising fields—spoof plasmonics [36]

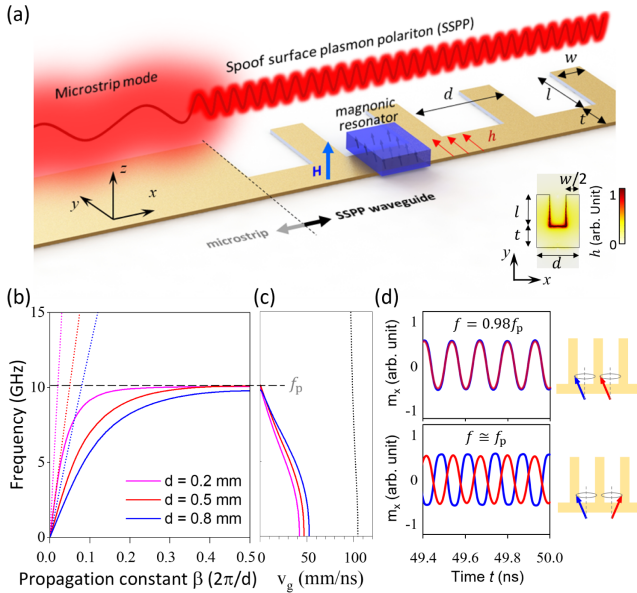


FIG. 1. (a) Schematics of the hybrid SSPP-magnonic device (not to scale). A planar magnonic resonator is placed on a periodically corrugated microstrip. Inset: simulated mode profile (total magnetic field h) of SSPPs. (b) Dispersions and (c) group velocities obtained from COMSOL simulation for SSPPs on a waveguide with $w = t = 100$ μm , $l = 3$ mm, and varying period d . Dotted lines: dispersions of the same uncorrugated microstrip, plotted against β values that are normalized using different d values. f_p : effective plasma frequency of SSPPs. (d) Phase-field simulation results for the temporal evolution of the precessing field m_x of the magnon modes in two neighboring magnonic resonators (in phase at $f = 0.98f_p$; π out of phase at $f \approx f_p$).

and cavity magnonics—and show that it can lead to broadband hybrid magnonic interactions while maintaining large coupling strengths, as well as enable complicated system dynamics that is of critical importance for complex magnonic systems such as magnonic crystals [39–43] and magnonic networks [44]. Furthermore, we demonstrate slow-wave strong coupling within our system, a phenomenon that has not been experimentally observed in magnonics or other systems.

Our slow-wave hybrid magnonic device consists of a conformal SSPP waveguide [45] and a magnonic resonator [Fig. 1(a)]. The SSPP waveguide is a metallic microstrip with periodic corrugations (period: d), which supports slowly propagating SSPPs that mimic optical surface plasmons at metal or dielectric interfaces. Figure 1(b) plots the simulated dispersion curves of the fundamental SSPP modes on the waveguide (solid lines), which dramatically deviate from the dispersion of the uncorrugated microstrip modes (dotted lines) because of their polaritonic nature [36]. At the edge of the first Brillouin zone where the propagation constant $\beta = \pi/d$, the SSPP dispersion becomes nearly flat and asymptotically approaches the effective plasma frequency f_p , where the group velocity is largely reduced [Fig. 1(c)].

The effective plasma frequency f_p of SSPPs is primarily determined by the corrugation depth l , which reaches around 10 GHz when $l = 3$ mm. The dispersion curve, and accordingly the group velocity, can be fine tuned by the corrugation period d without significantly affecting f_p [Figs. 1(b) and 1(c)]. The corrugation teeth width w has negligible effects and $w = 0.1$ mm is used throughout our experiments. The dispersion curve and f_p are also sensitive to the magnonic resonator chip (size, alignment, bonding condition) and thus may vary from device to device in our experiment.

As the SSPP frequency approaches f_p , the reduced group velocity is accompanied by the enhanced mode confinement [Fig. 1(a), inset], which can reach deep subwavelength level. The magnetic fields of SSPPs are strongly localized at the bottom of the corrugations, inducing enhanced coupling with magnons when planar magnonic resonators are placed there. The magnonic resonators are biased by an external magnetic field along z , which is perpendicular to the magnetic field (in y direction) of SSPPs to ensure their proper coupling with magnons. The strength of the bias field, which determines the magnon frequency, is controlled by the z position of the magnet using an automated stage.

The coherent SSPP-magnon coupling is confirmed by our phase-field simulation [46] based on coupled Maxwell's equations and Landau-Lifshitz-Gilbert equation [52,53]. Our simulation shows that when the frequencies of SSPPs and magnons match, the oscillating magnetic field of SSPPs excites the precessing magnetization of magnon (and vice versa) through magnetic dipole-dipole interaction, and the magnon phase is determined by the phase of SSPP. Therefore, if multiple magnonic resonators are placed in series on an SSPP waveguide, their relative phase can be tuned by varying the operation frequency which accordingly changes the propagation constant. Thanks to the nearly flat dispersion near f_p , a small frequency tuning can produce a large phase tuning. This is verified by the simulated temporal evolution of m_x [Fig. 1(d)], where the relative phase of two neighboring magnonic resonators (separated by d) varies from 0 to almost π when the frequency is tuned by 2%. Such a large phase tuning over a small distance is highly challenging when conventional waveguides such as microstrips or CPWs are used. The considerable phase tunability, enabled by the slow wave nature of SSPPs, presents a notable advantage over conventional resonator-based hybrid magnonic systems, where fixed phase detuning limits the system up scaling for intricate functionalities or dynamics, such as programmable interference within a sizable array of magnonic resonators.

The coupling strength between magnons and traveling SSPPs can be calculated using Fermi's golden rule

$$g_{\text{ms}} = 2\pi |g_0(\omega)|^2 D(\omega) = A \frac{\hbar\omega}{v_g S_{\text{eff}}}, \quad (1)$$

where $g_0(\omega) = (\gamma/2)\sqrt{(2\hbar\omega\mu_0sN/V)}$ is the single magnon-SSPP coupling rate, $D(\omega) = (L/2\pi v_g)$ is the density of state of the SSPPs traveling in one direction, and the coefficient $A = \frac{1}{2}\eta^2\gamma^2\mu_0sN$. Here \hbar is reduced Planck's constant, η is the mode overlapping factor [10], $\gamma = 28$ GHz/T is the gyromagnetic ratio, ω is the magnon angular frequency, s is the spin quantum number, μ_0 is the vacuum permeability, N is the total number of spins, $V = S_{\text{eff}} \times L$ is the effective interacting mode volume, S_{eff} is the effective cross-section area of the traveling SSPPs, L is the length of the YIG resonator, and $v_g = d\omega/d\beta$ is the group velocity of the traveling SSPPs. Compared with uncorrugated microstrips (width: $l + t$), SSPPs on our corrugated microstrip have significantly reduced mode cross-section area and group velocity [46], which will therefore lead to drastically increased coupling strengths between magnons and the microwave photons in the SSPP mode.

In our experiment, an SSPP waveguide with a 500 μm corrugation period is fabricated on a high-dielectric constant substrate ($\epsilon = 9.8$) [Fig. 2(a)]. Magnonic resonators (lateral sizes range from tens to hundreds of micrometers) are fabricated on a 200-nm thin film of ferrimagnetic insulator yttrium iron garnet (YIG) epitaxially grown on a 500- μm gadolinium gallium garnet (GGG) substrate. The magnonic chip is flip bonded to the SSPP waveguide circuit [Fig. 2(b)]. An out-of-plane bias magnetic field is applied

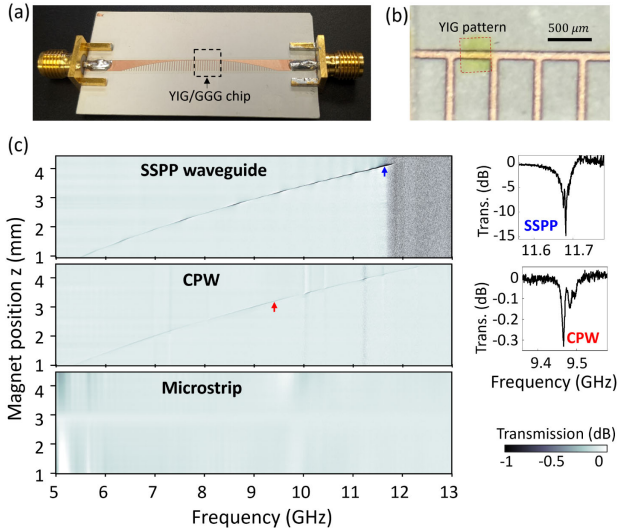


FIG. 2. (a) Optical image of the fabricated SSPP waveguide circuit. Between the SSPP waveguide and the SMA connectors there exists a tapered transition region where the corrugation depth l is quadratically varied. (b) Enlarged image showing a YIG resonator ($400 \mu\text{m} \times 400 \mu\text{m}$) flipped on the SSPP waveguide. (c) Measured transmission spectra for SSPP waveguide, CPW, and microstrip, respectively. Background spectra are removed to highlight the weak magnon resonances. Insets: the measured spectra corresponding to the points indicated by the arrows, respectively.

using a permanent magnet, which can be moved along the z direction to control the magnon frequency.

The transmission signals measured using a vector network analyzer on a device having a $400 \mu\text{m} \times 400 \mu\text{m} \times 200 \text{nm}$ YIG resonator is plotted in Fig. 2(c). As a comparison, transmissions from a CPW (width of center line: 100 μm , gap to the ground: 500 μm) and a uncorrugated microstrip (width: 3 mm) loaded with the same YIG resonator are also plotted. In all spectra, the transmission background is removed to reveal the small magnon absorption dips, which are observed in a broad frequency range (> 7 GHz). A maximum extinction ratio of 15 dB is obtained at 11.68 GHz (near f_p), whereas on the CPW it is 2 orders of magnitude smaller (0.3 dB at 9.46 GHz for the same magnon mode). On the uncorrugated microstrip, magnon modes are not observed. These results indicate the drastically enhanced SSPP-magnon interaction due to the small group velocity of SSPPs, which is highly advantageous over CPWs or microstrips particularly for miniaturized magnonic devices.

The slow wave enhancement of the SSPP-magnon coupling has a strong frequency dependence, as shown by the transmission spectra [Fig. 3(a)] for different magnon frequencies (determined by the magnet position z) on a device with a $300 \mu\text{m} \times 1000 \mu\text{m} \times 200 \text{nm}$ YIG resonator. When the magnet is at $z = 0$ mm, the magnon mode is absent and the spectrum shows the intrinsic characteristics of SSPPs: a broad transmission band with a cutoff at around 10 GHz ($\approx f_p$). Below the cutoff frequency, an insertion loss of about 12 dB is measured, which is attributed to the metal

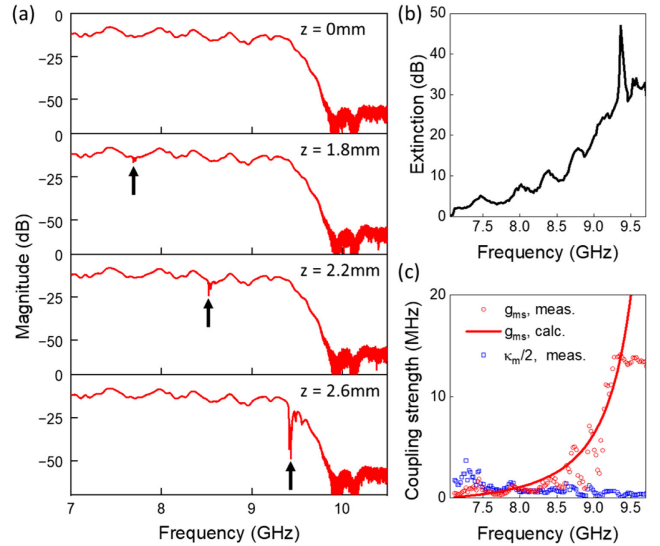


FIG. 3. (a) Measured transmission spectra of the SSPP waveguide with the magnet at different positions z . Black arrows indicate the magnon resonances. (b) Extracted extinction ratio of the magnon resonances as a function of the magnon frequency. (c) Extracted (red circles) and calculated (solid line) SSPP-magnon coupling strength g_{ms} as a function of magnon frequency. Blue squares: extracted intrinsic magnon damping rate $\kappa_m/2$.

absorption and coupling loss with the rf connectors, while above the cutoff frequency, the transmission drops to below -50 dB because SSPPs are no longer supported. When the bias magnet moves towards the device, magnon modes are observed over a broad frequency range as narrow absorption dips in the transmission spectrum. For instance, when the magnet is at $z = 1.8$ mm, magnon resonances are visible at 7.7 GHz, which further increases to 8.5 GHz at $z = 2.2$ mm and 9.4 GHz at $z = 2.6$ mm, respectively.

Figure 3(a) reveals one striking feature of these magnon resonances: their extinction ratio increases as the magnon frequency approaches the SSPP cutoff frequency. Such dependence is clearly shown by the extracted extinction ratio as a function of the magnon frequency [Fig. 3(b)]. The small oscillations in the curve are due to the interference effects of the SSPPs when propagating along the waveguide with a finite length, but they are much weaker than the enhancement effect caused by the increased magnon frequency. A maximum extinction ratio of 47 dB is observed at the edge of the cutoff frequency ($z = 2.6$ mm), which is more than four orders of magnitude higher than what is obtained near $z = 1.8$ mm.

The SSPP-magnon coupling strength [Fig. 3(c), red circles] is extracted from the measured spectra [46]. Despite the fluctuation caused by the background interference (8.5–9 GHz) [46], an increasing trend with magnon frequency is evident. Because $S_{\text{eff}} \propto 1/\beta^2$ [46], Eq. (1) can be rewritten as $g_{\text{ms}} = A'\omega\beta^2/v_g$, where the phenomenological coefficient A' is the only unknown parameter since both the dispersion $\beta(\omega)$ and group velocity $v_g(\omega)$ can be obtained from simulations. Good agreement is obtained between our theoretical calculation [solid line in Fig. 3(c)] and the measurement results, with an exception above 9.3 GHz where the reduced transmission causes inaccurate numerical fittings. A maximum SSPP-magnon coupling strength of nearly 15 MHz are measured at 9.2 GHz, which is 20 times larger than the extracted intrinsic magnon damping rate $\kappa_m/2 = 0.7$ MHz. Even larger coupling strengths are expected, but their observation is hindered by the increased SSPP loss (accordingly, transmission drop) near f_p .

Similar to cavity hybrid magnonics, SSPP-magnon coupling can be enhanced by increasing the YIG volume. Figure 4 plots the measured transmission for a $5 \text{ mm} \times 5 \text{ mm} \times 3 \text{ }\mu\text{m}$ YIG resonator on the same SSPP waveguide. An anti-crossing feature with a splitting $2g_{\text{ms}} = 0.7$ GHz is observed near the cutoff frequency around 8.4 GHz [Fig. 4(b)]. This is modeled based on the frequency response of YIG's permeability near the magnonic resonance and its effect on the effective plasma frequency of SSPPs. The theoretical prediction shows great agreement with the measurement results [Fig. 4(a)], with all four curves computed concurrently using a single equation involving only two fitting parameters [46]. The coupling strength $g_{\text{ms}} = 0.35$ GHz corresponds to an oscillation

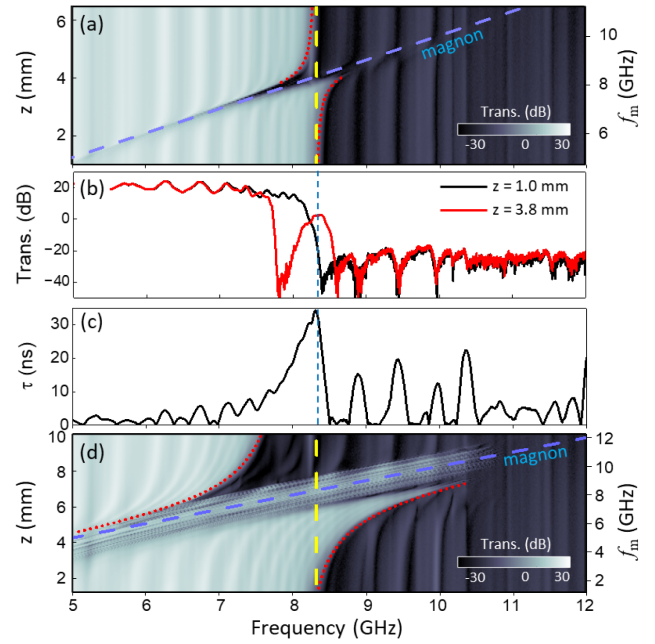


FIG. 4. (a) Measured transmission spectra of a SSPP waveguide covered by $5 \text{ mm} \times 5 \text{ mm} \times 3 \text{ }\mu\text{m}$ rectangular YIG resonator. (b) The measured SSPP waveguide transmission at magnet position $z = 1.0$ mm (black) and $z = 3.8$ mm (red), respectively. (c) Extracted group delay τ from the measured transmission phase. The large oscillations above the cutoff frequency are due to standing waves. (d) The measured transmission spectra using a $350\text{-}\mu\text{m}$ -thick, 5-mm -diameter YIG disc. Trans.: transmission. All dashed and dotted lines in (a) and (d) are from calculation and use the y axis on the right. Blue line: calculated magnon mode; red and yellow lines: calculated f_p with and without SSPP-magnon coupling, respectively. f_m is the magnon frequency.

period $1/g_{\text{ms}} = 2.9$ ns for the coherent information exchange between magnons and SSPPs. On the other hand, the measured group delay $\tau = d\phi/d\omega$ of the whole 35-mm -long SSPP waveguide reaches a maximum of 32 ns [Fig. 4(c)], yielding a traveling time $\tau_g = 4.6$ ns for the SSPPs to pass the YIG resonator. Since the traveling time exceeds the oscillation period, the coherent signal will experience multiple oscillations between the magnon and SSPP modes while traveling through the interaction region, which can be defined as the slow-wave strong coupling condition: $\tau_g > 1/g_{\text{ms}}$. By replacing the $3\text{-}\mu\text{m}$ -thick YIG resonator with a thick YIG disc (thickness: $350 \text{ }\mu\text{m}$, diameter: 5 mm), the slow-wave SSPP-magnon strong coupling can be further enhanced with a splitting of 3.2 GHz ($g_{\text{ms}} = 1.6$ GHz) as obtained through our modeling [Fig. 4(d)], leading to a single-spin coupling strength $g_0 = 130$ Hz. Considering that $g_{\text{ms}}/f_p = 19.3\%$, this corresponds to the ultrastrong coupling in conventional hybrid magnonics.

This Letter demonstrates a novel type of slow-wave hybrid magnonics based on SSPP-magnon interaction. Thanks to the small group velocities of the SSPPs, our

device platform exhibits significantly enhanced coupling strength while maintaining a large operation bandwidth, combining the advantages of cavity magnonics and traveling wave devices. Our slow-wave hybrid magnonic system opens a new chapter for hybrid magnonics, promising potential applications in integrated magnonic circuits [54,55] and quantum information processing [6,56–61]. Moreover, our demonstrated principle can be extended to other hybrid magnonic systems such as optomagnonics and magnomechanics. This Letter also points to a new direction for the study and application of spoof plasmonics.

The authors thank R. Divan, L. Stan, and C. Miller for supports in the device fabrication. X.Z. acknowledges support from Office of Naval Research Young Investigator Award (N00014-23-1-2144). C.Z. and L.J. acknowledge support from the ARO (W911NF-23-1-0077), AFRL (FA8649-21-P-0781), NSF (OMA-2137642), NTT Research, and Packard Foundation (2020-71479). L.J. acknowledges the support from the Marshall and Arlene Bennett Family Research Program. J.H. acknowledges support from the National Science Foundation (NSF) Award No. CBET-2006028. The works on dynamical phase-field simulations used Bridges2-GPU at Pittsburgh Supercomputing Center through allocation DMR180076 from the Advanced Cyberinfrastructure Coordination Ecosystem: Services & Support (ACCESS) program, which is supported by National Science Foundation (Grant No. 2138259, No. 2138286, No. 2138307, No. 2137603, and No. 2138296). J.M.J. acknowledges funding support from the US National Science Foundation (Grant No. 2011411). Work performed at the Center for Nanoscale Materials, a U.S. Department of Energy Office of Science User Facility, was supported by the U.S. DOE, Office of Basic Energy Sciences, under Contract No. DE-AC02-06CH11357.

*xu.zhang@northeastern.edu

- [1] B. Z. Rameshti, S. V. Kusminskiy, J. A. Haigh, K. Usami, D. Lachance-Quirion, Y. Nakamura, C.-M. Hu, H. X. Tang, G. E. Bauer, and Y. M. Blanter, Cavity magnonics, *Phys. Rep.* **979**, 1 (2022).
- [2] M. Harder and C.-M. Hu, Cavity spintronics: An early review of recent progress in the study of magnon–photon level repulsion, *Solid State Phys.* **69**, 47 (2018).
- [3] D. Lachance-Quirion, Y. Tabuchi, A. Gloppe, K. Usami, and Y. Nakamura, Hybrid quantum systems based on magnonics, *Appl. Phys. Express* **12**, 070101 (2019).
- [4] B. Bhoi and S.-K. Kim, Roadmap for photon-magnon coupling and its applications, in *Solid State Physics* (Elsevier, New York, 2020), Vol. 71, pp. 39–71, [10.1016/bs.ssp.2020.09.004](https://doi.org/10.1016/bs.ssp.2020.09.004).
- [5] Y. Li, W. Zhang, V. Tyberkevych, W.-K. Kwok, A. Hoffmann, and V. Novosad, Hybrid magnonics: Physics, circuits, and applications for coherent information processing, *J. Appl. Phys.* **128**, 130902 (2020).
- [6] D. D. Awschalom, C. R. Du, R. He, F. J. Heremans, A. Hoffmann, J. Hou, H. Kurebayashi, Y. Li, L. Liu, V. Novosad *et al.*, Quantum engineering with hybrid magnonic systems and materials, *IEEE Trans. Quantum Eng.* **2**, 1 (2021).
- [7] A. A. Serga, A. V. Chumak, and B. Hillebrands, YIG magnonics, *J. Phys. D* **43**, 264002 (2010).
- [8] A. V. Chumak, Magnon spintronics: Fundamentals of magnon-based computing, in *Spintronics Handbook*, Second Edition: Spin Transport and Magnetism (CRC Press, Boca Raton, FL, USA, 2019), pp. 247–302.
- [9] H. Huebl, C. W. Zollitsch, J. Lotze, F. Hocke, M. Greifenstein, A. Marx, R. Gross, and S. T. B. Goennenwein, High cooperativity in coupled microwave resonator ferrimagnetic insulator hybrids, *Phys. Rev. Lett.* **111**, 127003 (2013).
- [10] X. Zhang, C.-L. Zou, L. Jiang, and H. X. Tang, Strongly coupled magnons and cavity microwave photons, *Phys. Rev. Lett.* **113**, 156401 (2014).
- [11] Y. Tabuchi, S. Ishino, T. Ishikawa, R. Yamazaki, K. Usami, and Y. Nakamura, Hybridizing ferromagnetic magnons and microwave photons in the quantum limit, *Phys. Rev. Lett.* **113**, 083603 (2014).
- [12] M. Goryachev, W. G. Farr, D. L. Creedon, Y. Fan, M. Kostylev, and M. E. Tobar, High-cooperativity cavity QED with magnons at microwave frequencies, *Phys. Rev. Appl.* **2**, 054002 (2014).
- [13] L. Bai, M. Harder, Y. P. Chen, X. Fan, J. Q. Xiao, and C.-M. Hu, Spin pumping in electro-dynamically coupled magnon-photon systems, *Phys. Rev. Lett.* **114**, 227201 (2015).
- [14] J. T. Hou and L. Liu, Strong coupling between microwave photons and nanomagnet magnons, *Phys. Rev. Lett.* **123**, 107702 (2019).
- [15] Y. Li, V. G. Yefremenko, M. Lisovenko, C. Trevillian, T. Polakovic, T. W. Cecil, P. S. Barry, J. Pearson, R. Divan, V. Tyberkevych, C. L. Chang, U. Welp, W.-K. Kwok, and V. Novosad, Coherent coupling of two remote magnonic resonators mediated by superconducting circuits, *Phys. Rev. Lett.* **128**, 047701 (2022).
- [16] Y.-P. Wang, J. W. Rao, Y. Yang, P.-C. Xu, Y. S. Gui, B. M. Yao, J. Q. You, and C.-M. Hu, Nonreciprocity and unidirectional invisibility in cavity magnonics, *Phys. Rev. Lett.* **123**, 127202 (2019).
- [17] X. Zhang, A. Galda, X. Han, D. Jin, and V. M. Vinokur, Broadband nonreciprocity enabled by strong coupling of magnons and microwave photons, *Phys. Rev. Appl.* **13**, 044039 (2020).
- [18] R. Hisatomi, A. Osada, Y. Tabuchi, T. Ishikawa, A. Noguchi, R. Yamazaki, K. Usami, and Y. Nakamura, Bidirectional conversion between microwave and light via ferromagnetic magnons, *Phys. Rev. B* **93**, 174427 (2016).
- [19] N. Zhu, X. Zhang, X. Han, C.-L. Zou, C. Zhong, C.-H. Wang, L. Jiang, and H. X. Tang, Waveguide cavity optomagnonics for microwave-to-optics conversion, *Optica* **7**, 1291 (2020).
- [20] N. Crescini, D. Alesini, C. Braggio, G. Carugno, D. D’Agostino, D. Di Gioacchino, P. Falferi, U. Gambardella, C. Gatti, G. Iannone, C. Ligi, A. Lombardi, A. Ortolan, R. Pengo, G. Ruoso, and L. Taffarello (QUAX

- Collaboration), Axion search with a quantum-limited ferromagnetic haloscope, *Phys. Rev. Lett.* **124**, 171801 (2020).
- [21] G. Flower, J. Bourhill, M. Goryachev, and M. E. Tobar, Broadening frequency range of a ferromagnetic axion haloscope with strongly coupled cavity-magnon polaritons, *Phys. Dark Universe* **25**, 100306 (2019).
- [22] L. Millet, H. Jeon, B. Kim, B. Bhoi, and S.-K. Kim, Reservoir computing using photon-magnon coupling, *Appl. Phys. Lett.* **119**, 182405 (2021).
- [23] J. Bourhill, N. Kostylev, M. Goryachev, D. L. Creedon, and M. E. Tobar, Ultrahigh cooperativity interactions between magnons and resonant photons in a YIG sphere, *Phys. Rev. B* **93**, 144420 (2016).
- [24] I. A. Golovchanskiy, N. N. Abramov, V. S. Stolyarov, M. Weides, V. V. Ryazanov, A. A. Golubov, A. V. Ustinov, and M. Y. Kupriyanov, Ultrastrong photon-to-magnon coupling in multilayered heterostructures involving superconducting coherence via ferromagnetic layers, *Sci. Adv.* **7**, eabe8638 (2021).
- [25] X. Zhang, C.-L. Zou, L. Jiang, and H. X. Tang, Cavity magnomechanics, *Sci. Adv.* **2**, e1501286 (2016).
- [26] X. Zhang, N. Zhu, C.-L. Zou, and H. X. Tang, Optomagnonic whispering gallery microresonators, *Phys. Rev. Lett.* **117**, 123605 (2016).
- [27] A. Osada, R. Hisatomi, A. Noguchi, Y. Tabuchi, R. Yamazaki, K. Usami, M. Sadgrove, R. Yalla, M. Nomura, and Y. Nakamura, Cavity optomagnonics with spin-orbit coupled photons, *Phys. Rev. Lett.* **116**, 223601 (2016).
- [28] J. A. Haigh, A. Nunnenkamp, A. J. Ramsay, and A. J. Ferguson, Triple-resonant Brillouin light scattering in magneto-optical cavities, *Phys. Rev. Lett.* **117**, 133602 (2016).
- [29] B. Bhoi, S.-H. Jang, B. Kim, and S.-K. Kim, Broadband photon-magnon coupling using arrays of photon resonators, *J. Appl. Phys.* **129** (2021).
- [30] T. Sebastian, K. Schultheiss, B. Obry, B. Hillebrands, and H. Schultheiss, Micro-focused Brillouin light scattering: Imaging spin waves at the nanoscale, *Front. Phys.* **3**, 35 (2015).
- [31] K. H. Jensen, M. N. Alam, B. Scherer, A. Lambrecht, and N. A. Mortensen, Slow-light enhanced light-matter interactions with applications to gas sensing, *Opt. Commun.* **281**, 5335 (2008).
- [32] L. Thévenaz, I. Dicaire, and S. Chin, Enhancing the light-matter interaction using slow light: Towards the concept of dense light, in *Proceedings Volume 8273, Advances in Slow and Fast Light V* (SPIE, 2012), Vol. 8273, pp. 193–200.
- [33] X. Zang, J. Yang, R. Faggiani, C. Gill, P. G. Petrov, J.-P. Hugonin, K. Vynck, S. Bernon, P. Bouyer, V. Boyer, and P. Lalanne, Interaction between atoms and slow light: A study in waveguide design, *Phys. Rev. Appl.* **5**, 024003 (2016).
- [34] G. Calajo and P. Rabl, Strong coupling between moving atoms and slow-light Cherenkov photons, *Phys. Rev. A* **95**, 043824 (2017).
- [35] J. B. Pendry, L. Martín-Moreno, and F. J. Garcia-Vidal, Mimicking surface plasmons with structured surfaces, *Science* **305**, 847 (2004).
- [36] Z. Gao, L. Wu, F. Gao, Y. Luo, and B. Zhang, Spoof plasmonics: From metamaterial concept to topological description, *Adv. Mater.* **30**, 1706683 (2018).
- [37] W. X. Tang, H. C. Zhang, H. F. Ma, W. X. Jiang, and T. J. Cui, Concept, theory, design, and applications of spoof surface plasmon polaritons at microwave frequencies, *Adv. Opt. Mater.* **7**, 1800421 (2019).
- [38] F. J. Garcia-Vidal, A. I. Fernández-Domínguez, L. Martín-Moreno, H. C. Zhang, W. Tang, R. Peng, and T. J. Cui, Spoof surface plasmon photonics, *Rev. Mod. Phys.* **94**, 025004 (2022).
- [39] A. V. Chumak, A. A. Serga, and B. Hillebrands, Magnonic crystals for data processing, *J. Phys. D* **50**, 244001 (2017).
- [40] A. De, S. Mondal, S. Choudhury, S. Sahoo, S. Majumder, S. Barman, Y. Otani, and A. Barman, Shape dependent high frequency spin-wave dynamics in nanoscale magnonic crystals, *J. Magn. Magn. Mater.* **487**, 165263 (2019).
- [41] A. De, K. Dutta, S. Mondal, S. Barman, Y. Otani, and A. Barman, Magnonic crystals with complex geometry, *Phys. Rev. B* **103**, 064402 (2021).
- [42] P. K. Pal, S. Majumder, Y. Otani, and A. Barman, Bias-field tunable magnon-magnon coupling in Ni₈OFe₂O nanocross array, *Adv. Quantum Technol.* **6**, 2300003 (2023).
- [43] A. Adhikari, S. Majumder, Y. Otani, and A. Barman, Active control of dipole-exchange coupled magnon modes in nanoscale bicomponent magnonic crystals, *ACS Appl. Nano Mater.* **6**, 7166 (2023).
- [44] Y. V. Khivintsev, V. K. Sakharov, A. V. Kozhevnikov, G. M. Dudko, Y. A. Filimonov, and A. Khitun, Spin waves in YIG based magnonic networks: Design and technological aspects, *J. Magn. Magn. Mater.* **545**, 168754 (2022).
- [45] X. Shen, T. J. Cui, D. Martín-Cano, and F. J. Garcia-Vidal, Conformal surface plasmons propagating on ultrathin and flexible films, *Proc. Natl. Acad. Sci. U.S.A.* **110**, 40 (2013).
- [46] See Supplemental Material at <http://link.aps.org/supplemental/10.1103/PhysRevLett.132.116701> for details about device modeling, simulation, preparation, and measurements, which includes Refs. [45,47–52].
- [47] J.-M. Jin, *Theory and Computation of Electromagnetic Fields* (Wiley, 2010).
- [48] A. Taflové, S. C. Hagness, and M. Piket-May, Computational electromagnetics: The finite-difference time-domain method, in *The Electrical Engineering Handbook* (Elsevier Inc, München, Germany, 2005), pp. 629–670.
- [49] A. Kamra, H. Keshtgar, P. Yan, and G. E. W. Bauer, Coherent elastic excitation of spin waves, *Phys. Rev. B* **91**, 104409 (2015).
- [50] A. V. Azovtsev and N. A. Pertsev, Dynamical spin phenomena generated by longitudinal elastic waves traversing CoFe₂O₄ films and heterostructures, *Phys. Rev. B* **100**, 224405 (2019).
- [51] C. Liu *et al.*, Long-distance propagation of short-wavelength spin waves, *Nat. Commun.* **9**, 1 (2018).
- [52] S. Zhuang and J.-M. Hu, Excitation and detection of coherent sub-terahertz magnons in ferromagnetic and anti-ferromagnetic heterostructures, *npj Comput. Mater.* **8**, 1 (2022).
- [53] S. Zhuang and J.-M. Hu, Acoustic attenuation in magnetic insulator films: Effects of magnon polaron formation, *J. Phys. D* **56**, 054004 (2023).
- [54] Q. Wang, P. Pirro, R. Verba, A. Slavin, B. Hillebrands, and A. V. Chumak, Reconfigurable nanoscale spin-wave directional coupler, *Sci. Adv.* **4**, 7093 (2018).

- [55] Q. Wang, M. Kewenig, M. Schneider, R. Verba, F. Kohl, B. Heinz, M. Geilen, M. Mohseni, B. Lagel, F. Ciubotaru, C. Adelman, C. Dubs, S. D. Cotofana, O. V. Dobrovolskiy, T. Bracher, P. Pirro, and A. V. Chumak, A magnonic directional coupler for integrated magnonic half-adders, *Nature Electronics* **3**, 765 (2020).
- [56] Y. Tabuchi, S. Ishino, A. Noguchi, T. Ishikawa, R. Yamazaki, K. Usami, and Y. Nakamura, Coherent coupling between a ferromagnetic magnon and a superconducting qubit, *Science* **349**, 405 (2015).
- [57] D. Lachance-Quirion, Y. Tabuchi, A. Gloppe, K. Usami, and Y. Nakamura, Hybrid quantum systems based on magnonics, *Appl. Phys. Express* **12**, 070101 (2019).
- [58] D. Lachance-Quirion, S. P. Wolski, Y. Tabuchi, S. Kono, K. Usami, and Y. Nakamura, Entanglement-based single-shot detection of a single magnon with a superconducting qubit, *Science* **367**, 425 (2020).
- [59] T. Hirotsawa, A. Mook, J. Klinovaja, and D. Loss, Magnetolectric cavity magnonics in skyrmion crystals, *PRX Quantum* **3**, 040321 (2022).
- [60] H. Y. Yuan, Y. Cao, A. Kamra, R. A. Duine, and P. Yan, Quantum magnonics: When magnon spintronics meets quantum information science, *Phys. Rep.* **965**, 1 (2022).
- [61] D. Xu, X.-K. Gu, H.-K. Li, Y.-C. Weng, Y.-P. Wang, J. Li, H. Wang, S.-Y. Zhu, and J. Q. You, Quantum control of a single magnon in a macroscopic spin system, *Phys. Rev. Lett.* **130**, 193603 (2023).